This work was written as part of one of the author's official duties as an Employee of the United States Government and is therefore a work of the United States Government. In accordance with 17 U.S.C. 105, no copyright protection is available for such works under U.S. Law.

Public Domain Mark 1.0
https://creativecommons.org/publicdomain/mark/1.0/

Access to this work was provided by the University of Maryland, Baltimore County (UMBC) ScholarWorks@UMBC digital repository on the Maryland Shared Open Access (MD-SOAR) platform.

Please provide feedback

Please support the ScholarWorks@UMBC repository by emailing scholarworks-group@umbc.edu and telling us what having access to this work means to you and why it's important to you. Thank you.

Check for updates

JGR Atmospheres

RESEARCH ARTICLE
10.1029/2020JD033656

Stratospheric Impacts of Continuing CFC-11 Emissions Simulated in a Chemistry-Climate Model

Eric L. Fleming[1,2], Qing Liang[1], Luke D. Oman[1], Paul A. Newman[1], Feng Li[1,3], and Margaret M. Hurwitz[4]

[1]NASA Goddard Space Flight Center, Greenbelt, MD, USA, [2]Science Systems and Applications, Inc., Lanham, MD, USA, [3]Universities Space Research Association, Columbia, MD, USA, [4]NOAA National Weather Service, Forecast Services Division, Silver Spring, MD, USA

Key Points:

- Continuing trichlorofluoromethane (CFC-11) emissions will cause additional future stratospheric ozone depletion
- Largest statistically significant ozone depletion occurs in the global and Antarctic spring total column, and global upper stratosphere
- Additional ozone depletion due to continuing CFC-11 emissions will cause small changes in stratospheric temperature and circulation

Correspondence to:
E. L. Fleming,
eric.l.fleming@nasa.gov

Citation:
Fleming, E. L., Liang, Q., Oman, L. D., Newman, P. A., Li, F., & Hurwitz, M. M. (2021). Stratospheric impacts of continuing CFC-11 emissions simulated in a chemistry-climate model. *Journal of Geophysical Research: Atmospheres*, *126*, e2020JD033656. https://doi.org/10.1029/2020JD033656

Received 7 AUG 2020
Accepted 7 DEC 2020

© 2021. American Geophysical Union. All Rights Reserved. This article has been contributed to by US Government employees and their work is in the public domain in the USA.

Abstract Trichlorofluoromethane (CFC-11, $CFCl_3$) is a major anthropogenic ozone-depleting substance and greenhouse gas, and its production and consumption are controlled under the Montreal Protocol. However, recent studies show that CFC-11 emissions increased during 2014–2017 relative to 2008–2012. In this study, we use a chemistry-climate model to investigate the stratospheric impacts of potential CFC-11 emissions continuing into the future. As a sensitivity test, we use a high CFC-11 scenario in which the inferred 2013–2016 average emissions of 72.5 Gg/yr is sustained to year 2100. This increases equivalent effective stratospheric chlorine by 15% in 2100, relative to the WMO (2018) baseline scenario in which future emissions decay with a bank release rate of 6.4%/year. Consistent with recent studies, the resulting ozone response has a linear dependence on the accumulated CFC-11 emissions, yielding global and Antarctic spring total ozone sensitivity per 1,000 Gg of −0.37 and −3.9 DU, respectively, averaged over 2017–2100. The deepened ozone hole reduces UV heating, causing a colder Antarctic lower stratosphere in spring/early summer. Through thermal wind balance, this accelerates the circumpolar jet which in turn alters planetary and gravity wave propagation through the Southern Hemisphere stratosphere, and modifies the Brewer-Dobson circulation. Age of air in the high scenario is slightly younger than the baseline in the lower stratosphere globally during 2090–2099, with a maximum change of −0.1 years. Coupled atmosphere-ocean model simulations show that the resulting greenhouse gas impact of CFC-11 is small and not statistically significant throughout the troposphere and stratosphere.

1. Introduction

Chlorofluorocarbons (CFCs) are powerful ozone-depleting substances (ODSs) and greenhouse gases (GHGs). One of the most abundant CFCs is trichlorofluoromethane (CFC-11, $CFCl_3$), which historically was used in a variety of industrial applications. Because it depletes the ozone layer, CFC-11 production and consumption have been controlled under the Montreal Protocol and subsequent amendments, resulting in a dramatic decline in emissions starting in the late 1980s (Cunnold et al., 1997). As a result of this emissions decrease and 52-year lifetime (SPARC, 2013), tropospheric concentrations of CFC-11 peaked in about 1994, and have since been declining up to the present.

However, recent studies showed that CFC-11 emissions increased during 2013–2016, and this emissions increase was likely not explained by release from existing CFC-11 banks (Engel and Rigby, 2018; Montzka et al., 2018; Rigby et al., 2019). These studies suggest that the emissions increase was associated with new production and consumption not reported to the United Nations Environment Programme. Furthermore, in a detailed analysis of the banks and emissions of major CFCs, Lickley et al. (2020) found that the banks of CFC-11 and CFC-12 are likely substantially larger than assumed in recent WMO ozone assessment reports. This suggests that unless the banks can be captured and destroyed, future emissions of these CFCs subsequently will be larger than previously assumed. The causes and ramifications of the recent increase in CFC-11 emissions are also reported in WMO (2021).

Because CFC-11 has a long atmospheric residence time and significant potential to deplete ozone, the stratospheric response to present and potential future increases in CFC-11 emissions was investigated in several recent modeling studies (Dameris et al., 2019; Dhomse et al., 2019; Fleming et al., 2020; Keeble et al., 2020; WMO, 2021). A key finding of these studies was that a compact linear relationship exists between the cumulative CFC-11 emissions and the resulting ozone depletion and delay in ozone recovery, for both global

21698996, 2021, 9, Downloaded from https://agupubs.onlinelibrary.wiley.com/doi/10.1029/2020JD033656 by University Of Maryland, Wiley Online Library on [20/01/2023]. See the Terms and Conditions (https://onlinelibrary.wiley.com/terms-and-conditions) on Wiley Online Library for rules of use; OA articles are governed by the applicable Creative Commons License

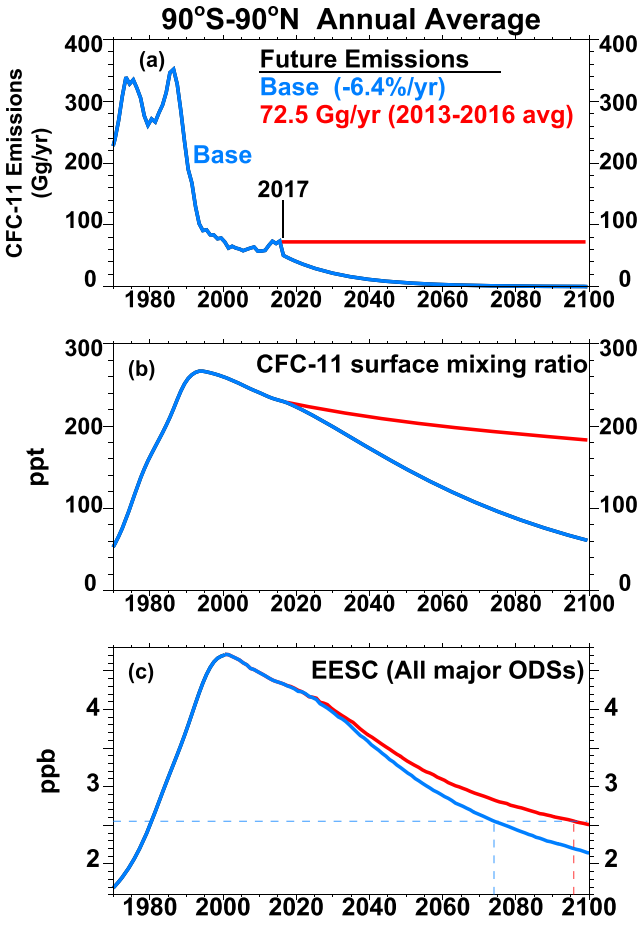

Figure 1. Global and annual average (a) CFC-11 surface emissions (Gigagrams (Gg)/year), (b) CFC-11 surface mixing ratio (parts-per-trillion (ppt)), and (c) upper stratospheric (50 km) equivalent effective stratospheric chlorine (EESC, parts-per-billion (ppb)). Shown are the baseline (blue) and "high" scenario assuming 72.5 Gg/yr sustained emissions for 2017–2100 (red). The scenarios are identical prior to 2017. The return dates to the 1980 EESC level are depicted by the dashed lines in panel (c). CFC-11, trichlorofluoromethane.

and Antarctic spring total ozone. A linear relationship was found across a range of future emissions scenarios and among several different models, although the sensitivity of the ozone response per unit emission varied among the models.

In this paper, we build on the aforementioned studies to further examine the stratospheric impacts due to potential CFC-11 emissions continuing into the future. Here, we use a three-dimensional (3-D) coupled chemistry-climate model (CCM) with well-resolved chemistry and dynamics, to further quantify and document the impact on equivalent effective stratospheric chlorine (EESC) and stratospheric ozone, and how the ozone response modifies stratospheric temperature, strength of the zonal jets, and the meridional Brewer-Dobson circulation (BDC). Although the stratospheric response to ODS loading has been well established in previous studies, here we provide a quantitative assessment of the impacts from a specific CFC-11 perturbation as a result of future emissions above that of current projections. Finally, since CFC-11 is also a powerful GHG (e.g., Hansen et al., 2005; Velders et al., 2007), we will examine the GHG impact on temperature, water vapor, and stratospheric age of air, using a coupled atmosphere-ocean CCM.

2. Model Simulations and Scenarios

The National Aeronautics and Space Administration (NASA) Goddard Earth Observing System 3-D chemistry climate model (GEOSCCM) is used for this study. The model has been used in numerous chemistry-climate coupling studies of the atmosphere, as well as the WMO ozone assessments, including WMO (2018). GEOSCCM uses the Global Modeling Initiative (GMI) detailed tropospheric and stratospheric chemical mechanism (Nielsen et al., 2017), and includes an internally generated QBO (Hurwitz et al., 2013). The model has performed well in process-oriented model intercomparisons (SPARC CCMVal, CCMVal-2, and Chemistry-Climate Modeling Initiative (CCMI); Chipperfield et al., 2014; Eyring et al., 2006, 2007; Eyring, Cionni, Bodeker, et al., 2010; Eyring, Cionni, Lamarque, et al., 2010). The JPL-2010 recommendations (Sander et al., 2011) are used for the kinetic reaction rates, photolysis cross sections, and heterogeneous reactions on the surfaces of stratospheric sulphate aerosols and polar stratospheric clouds (PSCs). The microphysical model for type I (nitric acid trihydrate, NAT) and type II (Ice) PSC formation follows Considine et al. (2000). Simulations are run at 2°×2° horizontal resolution, with 72 layers in the vertical, extending from the surface to 0.01 hPa (~80 km).

Two simulations are conducted in this study to examine the ozone depletion impacts of additional CFC-11. The SPARC CCMI REF-C2 simulation is used as the baseline for 1960–2100 (Dhomse et al., 2018; Eyring et al., 2013; Morgenstern et al., 2017). This simulation was also used for WMO (2018) and includes several time dependent forcings, listed as follows: the A1 scenario from WMO (2014) for surface mixing ratios of the major long lived ODS; the Coupled Model Intercomparison Project (CMIP) Representative Concentration Pathways (RCP) medium Scenario 6.0 ("historic" scenario before 2005, Meinshausen et al., 2011) for surface mixing ratios of CO_2, CH_4, and N_2O; stratospheric sulphate aerosol surface area density for background and volcanically active periods during 1960–2010, and background conditions projected to 2100, from the International Global Atmospheric Chemistry (IGAC) data set (Morgenstern et al., 2017); specified sea surface temperature and sea ice concentrations (Morgenstern et al., 2017); 5 ppt additional stratospheric bromine from the very short-lived substances CH_2Br_2 and $CHBr_3$; tropospheric ozone precursor emissions; and solar ultraviolet flux variability associated with the 11-year solar cycle, using daily historical spectral-

21698996, 2021, 9, Downloaded from https://agupubs.onlinelibrary.wiley.com/doi/10.1029/2020JD033656 by University Of Maryland, Wiley Online Library on [20/01/2023]. See the Terms and Conditions (https://onlinelibrary.wiley.com/terms-and-conditions) on Wiley Online Library for rules of use; OA articles are governed by the applicable Creative Commons License

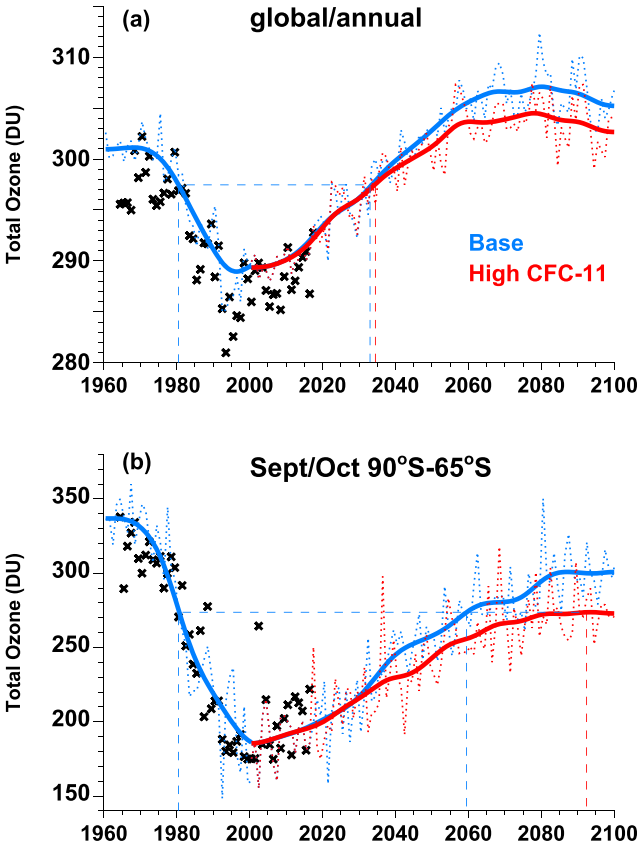

Figure 2. Total column ozone (Dobson Units, DU) for the (a) global (90°S–90°N) and annual average and (b) Antarctic spring (September–October, 65°S–90°S) average for the baseline (blue) and high (red) CFC-11 scenarios shown in Figure 1. Dotted colored lines show the unsmoothed time series; heavy solid colored lines show the smoothed time series after applying a 24-year ½ amplitude Gaussian smoothing. Also shown are the return dates to 1980 values (vertical dashed lines), and ground-based observations for 1964–2017 (black x's, updated from Fioletov et al., 2002). The model in (b) has been offset by −30 DU to minimize differences with the observations in the 1960s and facilitate model-data comparison of the long term changes. CFC-11, trichlorofluoromethane.

ly resolved solar irradiance data from the NRLSSI model for 1960–2018 (Lean et al., 2005). A repeating 11-year cycle is projected to 2100, using a composite average of solar cycles 21–24 (covering the period 1976–2018). For the baseline CFC-11 scenario, historic emissions are derived from global mixing ratio observations using a global one-box model (Velders & Daniel, 2014) and a fixed lifetime of 52 years (SPARC, 2013). Future emissions are projected to decay 6.4%/year; this assumes no new production and a bank release rate of 6.4%/year based on estimates of the amount of CFC-11 in existing equipment or applications (Harris & Wuebbles, 2014). The baseline emissions time series is shown in Figure 1a (blue line). Future global mixing ratios (Figure 1b, blue line) are computed from the emissions using a global one-box model assuming a constant 52-year lifetime (Harris & Wuebbles, 2014).

Our second simulation is a "high" CFC-11 scenario that assumes the 2013–2016 inferred average of 72.5 Gg/year will be sustained to year 2100 (Figure 1a, red line), but is otherwise identical to the baseline. While future CFC-11 emissions are projected to decrease from present day, assuming compliance with the Montreal Protocol and assuming that bank fractional release amounts remain roughly constant over time, the actual inferred emissions from atmospheric observations were fairly constant starting in 2002, and actually increased during 2013–2016 (Montzka et al., 2018; WMO, 2018). This 72.5 Gg/year emission level is slightly higher (by ~8%) than the longer term 2002–2016 inferred average of 67 Gg/year used in the recent WMO ozone assessment (Carpenter & Daniel, 2018; Engel & Rigby, 2018). For this high scenario, the GEOSCCM was forced with global average CFC-11 surface mixing ratios for 2017–2100. These were taken from a GSFC2D model simulation that used constant global average emissions of 72.5 Gg/year sustained to 2100 (Fleming et al., 2020), with a latitudinal emissions distribution based on industrial information (Liang et al., 2008; McCulloch et al., 2001). The baseline and high scenarios use identical surface mixing ratios prior to 2017.

We note that there is large uncertainty in future CFC-11 emissions, and the high scenario is not meant to be a realistic simulation, but rather is a sensitivity test of the stratospheric ozone and dynamics response. While 72.5 Gg/yr is defined as a high scenario based on previously reported emissions estimates, recent findings suggest that future CFC-11 emissions are likely to be substantially higher than previous estimates due to: (1) a substantially larger bank estimate (Lickley et al., 2020); and (2) potential newly formed banks related to recent unreported production and consumption of CFC-11 in east Asia (Park et al., 2021). As mentioned above, the actual response will be roughly proportional to the amount of increased future emissions incurred, based on the linearity of the response as shown in recent studies

CFC-11 is a powerful GHG, and both simulations include CFC-11 in the thermal infrared (IR) radiative transfer calculations. However, previous studies have shown the importance of sea surface temperature feedback on the stratospheric circulation response to radiative forcing (e.g., Olsen et al., 2007). Therefore, the full GHG impact of CFC-11 will be underestimated in these simulations, as they both use the same specified sea surface temperatures.

To examine more fully the impacts of CFC-11 as a GHG, we will also present results from previous simulations of a coupled atmosphere-ocean version of the GEOSCCM (Li et al., 2016, 2018). The ocean model is the Modular Ocean Model version 4p1 (Griffies, 2010) with approximately 1°×1° horizontal resolution and 50 layers. This version of the GEOSCCM uses the Rapid Radiative Transfer Model for General Circulation Model Applications (RRTMG; Mlawer et al., 1997; Iacono et al., 2000) IR radiation scheme to calculate the radiative forcing of CO_2, CH_4, N_2O, ozone, water vapor, and several halogenated compounds, including

21698996, 2021, 9, Downloaded from https://agupubs.onlinelibrary.wiley.com/doi/10.1029/2020JD033656 by University Of Maryland, Wiley Online Library on [20/01/2023]. See the Terms and Conditions (https://onlinelibrary.wiley.com/terms-and-conditions) on Wiley Online Library for rules of use; OA articles are governed by the applicable Creative Commons License

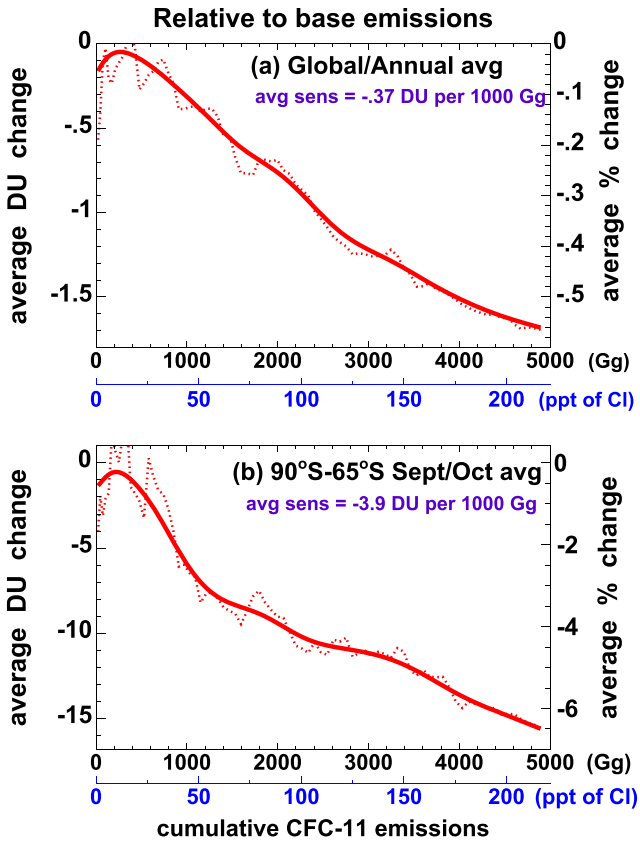

Figure 3. Average total ozone response versus cumulative CFC-11 emissions (high scenario – baseline) during 2017–2020 for the (a) global (90°S–90°N) and annual average, and (b) Antarctic spring (September–October, 65°S–90°S) average. Shown are the unsmoothed (dotted red line) and smoothed time series after applying a 24-year ½ amplitude Gaussian smoothing (heavy red line) as in Figure 2; the ozone response is lagged by 5 years to account for the time delay from emissions release at the surface and ozone depletion in the stratosphere. The total ozone sensitivity averaged over 2017–2100 is shown in the upper right corner. Cumulative emissions are expressed in both gigagrams (Gg) and parts per trillion (ppt) of chlorine, with the conversion from mass to volume mixing ratio done as in the 1-box model (Velders & Daniel, 2014). CFC-11, trichlorofluoromethane.

CFC-11. The baseline follows from a 170 year ocean spin-up simulation using perpetual 1950 conditions for the major GHGs and ODSs. The perturbation simulation is identical to the baseline, except CFC-11 with a very high surface mixing ratio (17.3 ppb) is used in the RRTMG IR code, while CFC-11 with a fixed 1950 baseline surface mixing ratio (0.001 ppb) is used in the ozone chemistry. The 17.3 ppb of CFC-11 corresponds to a radiative forcing of 4.5 W-m^{-2}, roughly the same as doubling the 1950 level of CO_2. To apply these results to this study, we assume the response is linear and scale the response by the CFC-11 perturbation mixing ratio in 2100 from Figure 1b (high scenario – base) versus 17.3 ppb (i.e., the response is scaled by the ratio 0.125 ppb/17.3 ppb). This corresponds to a radiative forcing of 0.0325 W-m^{-2}, assuming a CFC-11 radiative efficiency of 0.26 W-m^{-2}-ppb^{-1} (WMO, 2018). Section 3.3 shows results averaged over the final 10 years of this simulation, following a 50-year ocean spin-up phase in which sea surface temperatures adjust to the change in surface radiative forcing.

3. Results

3.1. Stratospheric Ozone and EESC Responses

The sustained 72.5 Gg/year scenario substantially perturbs the stratosphere. CFC-11 surface concentrations increase significantly through the 21st century to be 125 ppt above the baseline by 2100 (185 ppt vs. 60 ppt, Figure 1b), with a 0.35 ppb (15%) increase in global upper stratospheric (50 km) EESC (Figure 1c). The return of EESC to 1980 levels is delayed by 22 years (2074 vs. 2096).

21698996, 2021, 9, Downloaded from https://agupubs.onlinelibrary.wiley.com/doi/10.1029/2020JD033656 by University Of Maryland, Wiley Online Library on [20/01/2023]. See the Terms and Conditions (https://onlinelibrary.wiley.com/terms-and-conditions) on Wiley Online Library for rules of use; OA articles are governed by the applicable Creative Commons License

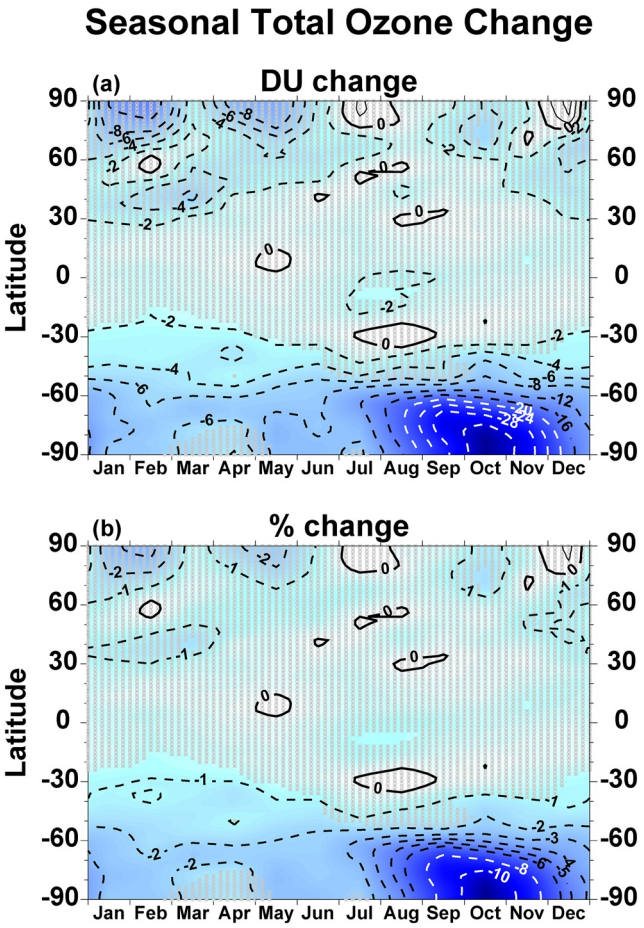

Figure 4. Total column ozone difference (high CFC-11 scenario – baseline) averaged over 2080–2100, expressed in (a) DU, and (b) percent. The contour intervals are: (a) ±2 DU for values ≥ −8, and −4 DU for values ≤ −8; (b) ±1 DU for values ≥ −6, and includes the −8 and −10 DU contours. Nonshaded regions indicate the response is statistically significant at the 95% level. CFC-11, trichlorofluoromethane.

Additional future ozone depletion results from the sustained 72.5 Gg/year emissions. Figure 2 shows total ozone responses for the (a) global and annual, and (b) Antarctic spring averages. Differences between the two simulations become apparent in the late 21st century in the smoothed time series (thick solid blue/red lines, using a Gaussian smoothing filter with a 24-year ½ amplitude). For the global average (Figure 2a), the high CFC-11 results in nearly 1% (2.8 Dobson units, DU) additional ozone depletion averaged over 2080–2100. Based on a two-sided Student's t-test, this is statistically significant at the 95% confidence level, i.e., the base and high scenarios have significantly different mean values for 2080–2100. This indicates that the additional global ozone depletion due to enhanced CFC-11 emissions is likely detectable above the model background variability (including the imposed 11-year solar cycle). Throughout Section 3, we will apply this significance test to determine the detectability of the model response to additional CFC-11.

The return of global ozone to 1980 levels is affected by the relatively strong increase in tropospheric ozone in GEOSCCM through the early mid-21st century (Dhomse et al., 2018). This, combined with the recovery in stratospheric ozone, yields a rather sharp increase in the total column during this time period so that the return of global total ozone to 1980 levels occurs fairly early in the GEOSCCM baseline (2033, blue vertical dashed line in Figure 2a). This is prior to the time period when the additional CFC-11 emissions have a significant impact on global total ozone. Therefore, the return to 1980 global ozone levels is delayed by only 1 year in the high CFC-11 scenario (2034 vs. 2033).

For Antarctic spring ozone (Figure 2b), the additional CFC-11 emissions results in 5.6% (19 DU) additional depletion averaged over 2080–2100, which is statistically significant at the 95% confidence level. The return to 1980 ozone levels is delayed by 33 years in the high scenario (2092 vs. 2059), as both scenarios show a leveling off of the ozone recovery after ~2080.

For reference, Figure 2 includes ground-based observations for 1964–2017 (black x's, updated from Fioletov et al., 2002), illustrating that the model reproduces overall the past long term changes observed since the 1960s. Note that the model in Figure 2b has been offset by −30 DU to minimize differences with the observations in the 1960s and facilitate model-data comparison of the long term changes.

As discussed in previous studies noted above, the future total ozone change integrated over time has a linear dependence on the accumulated CFC-11 emissions. This is seen in Figure 3, which shows the average total ozone change from Figure 2 (high scenario – baseline) plotted versus cumulative emissions for 2017–2100. Both the smoothed and unsmoothed time series are shown, and the ozone response is lagged by 5 years to account for the time delay between the emissions release at the surface and subsequent ozone depletion in the stratosphere. After ~2022, the ozone change versus cumulative emissions is mostly linear. Deviations from linearity are due in part to the model interannual variability, including the imposed 11-year solar cycle variation. While this linearity was seen in other recent modeling studies, the ozone change per unit emission varies somewhat across different models. For the global and annual average, the total ozone sensitivity averaged over 2017–2100 is −0.37 DU/1,000 Gg (Figure 3a). This is somewhat larger than the GSFC2D model sensitivity of −0.3 DU/1,000 Gg (Fleming et al., 2020), but weaker than the near-global (60°S–60°N) annual average of −0.7 to −0.9 DU/1,000 Gg from both the UM-UKCA CCM and the TOMCAT chemistry transport model (CTM) with specified meteorology and no chemistry-climate feedback (Keeble et al., 2020). For Antarctic spring, the GEOSCCM sensitivity (−3.9 DU/1,000 Gg, Figure 3b) is also larger than GSFC2D (−2.6 DU/1,000 Gg), but smaller than the TOMCAT CTM (~−6 DU/1,000 Gg, Dhomse et al., 2019).

21698996, 2021, 9, Downloaded from https://agupubs.onlinelibrary.wiley.com/doi/10.1029/2020JD033656 by University Of Maryland, Wiley Online Library on [20/01/2023]. See the Terms and Conditions (https://onlinelibrary.wiley.com/terms-and-conditions) on Wiley Online Library for rules of use; OA articles are governed by the applicable Creative Commons License

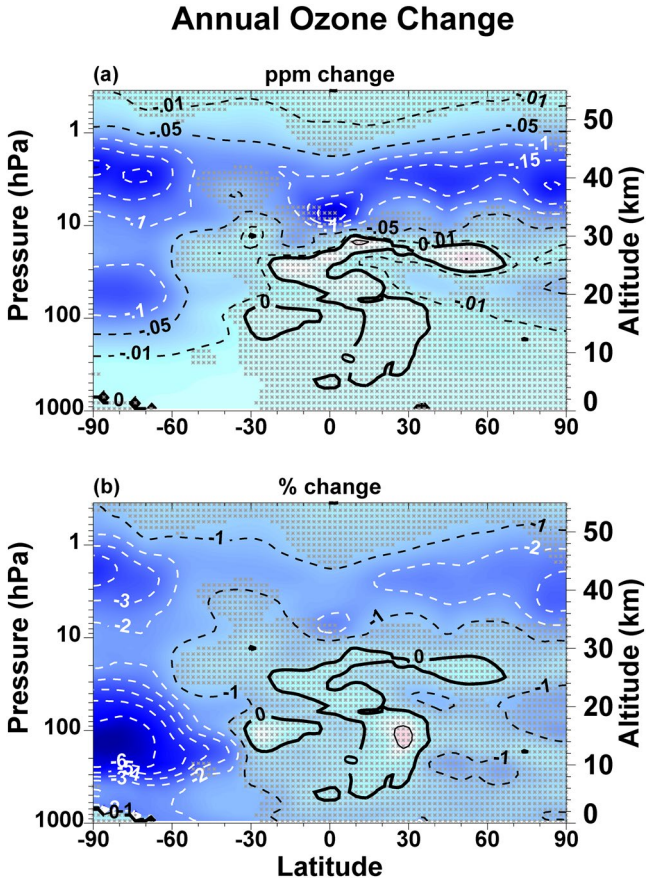

Figure 5. Ozone difference (high CFC-11 scenario – baseline) averaged over 2080–2100, expressed in: (a) parts-per-million (ppm), and (b) percent. The contours are: (a) ±0.05 ppm and includes the −0.01 contour; (b) ±1%. Nonshaded regions indicate the response is statistically significant at the 95% level. CFC-11, trichlorofluoromethane.

Additional ozone depletion from enhanced CFC-11 emissions is seasonally dependent. Figure 4 shows the 2080–2100 average seasonal versus latitude changes in total column ozone, expressed in DU (a) and percent (b). Maximum changes occur in the polar late winter and spring in each hemisphere, with relatively small changes at mid-latitudes and in the tropics. Generally similar distributions in the total ozone responses to CFC-11 perturbations were obtained in other recent modeling studies (Dameris et al., 2019; Fleming et al., 2020). The enhancement of depletion in the Antarctic ozone hole is evident in Figure 4, with an additional 12% (35 DU) of ozone loss during October. At Southern Hemisphere (SH) mid-high latitudes (30°S–90°S), the additional ozone depletion is statistically significant at the 95% level nearly the entire year. In the Northern Hemisphere (NH), the largest additional total ozone depletion of up to 2%–3% (8–10 DU) occurs in the polar mid-winter and spring (Figure 4), although this is not statistically significant given the large interannual variability inherent in the Arctic stratosphere during winter and spring. Therefore, the additional ozone depletion in the Arctic in this CFC-11 scenario would likely not be detectable above the background variability.

The latitude-height distribution of the ozone response to additional CFC-11 is consistent with that expected due to chlorine perturbations (e.g., WMO, 1999, 2018). Figure 5 shows the 2080–2100 annual average difference, high CFC-11 minus baseline, expressed in parts per million, ppm (a) and percent (b). The largest percentage ozone depletion occurs in the Antarctic lower stratosphere (−6 to −7%) and in the upper stratosphere globally (−1 to −4%). There is a secondary area of depletion of smaller magnitude in the Arctic lower stratosphere (−1%). Largest mixing ratio changes occur globally at 2–4 hPa (−0.1 to −0.2 ppm). The changes are statistically significant at the 95% confidence level throughout most of the SH stratosphere at mid-high latitudes, and in the upper stratosphere tropics and NH (Figure 5).

Maximum ozone depletion from the enhanced CFC-11 emissions occurs in the Antarctic ozone hole, with an additional −16% loss near 50 hPa in October. This is seen in the season versus altitude ozone change over the SH polar cap in Figure 6. This enhanced depletion develops in July–August and descends with time through the spring and summer. Figure 4 shows that additional depletion in total ozone of 2%–3% (6–8 DU) persists throughout the year at SH polar latitudes, and this reflects the profile ozone depletion at ~300–100 hPa (10–20 km) which is statistically significant at the 95% level throughout most of the year (Figure 6). Also contributing to the year-long total column change is the gas phase ozone loss caused by the additional chlorine in the upper stratosphere in Figure 6. Here, additional ozone depletion occurs throughout the year, although a maximum in depletion is evident during the winter months. There is also an area of ozone increase centered near 20 hPa during late spring and summer (November–February). This feature was discussed previously (Stolarski et al., 2006), and is caused by enhanced descent of the BDC in the mid-upper stratosphere associated with a dynamical response to the ozone hole. Although this positive ozone response in Figure 6 is not statistically significant at the 95% level, the associated temperature increase is statistically significant, as discussed in Section 3.2 and shown in Figure 10.

The additional ozone depletion associated with the ozone hole seen in Figure 5b extends to SH mid-latitudes in the lowermost stratosphere below 100 hPa. As shown in Figure 7, this depletion is especially large starting in late winter (August), and reaches a maximum of 5%–7% during spring and summer (September through February). There is also a broad area of 1%–2% additional depletion in the upper stratosphere during the austral spring, summer, and fall (September through early June). Most of the additional depletion in the lower and upper stratosphere at SH mid-latitudes is statistically significant at the 95% level.

21698996, 2021, 9, Downloaded from https://agupubs.onlinelibrary.wiley.com/doi/10.1029/2020JD033656 by University Of Maryland, Wiley Online Library on [20/01/2023]. See the Terms and Conditions (https://onlinelibrary.wiley.com/terms-and-conditions) on Wiley Online Library for rules of use; OA articles are governed by the applicable Creative Commons License

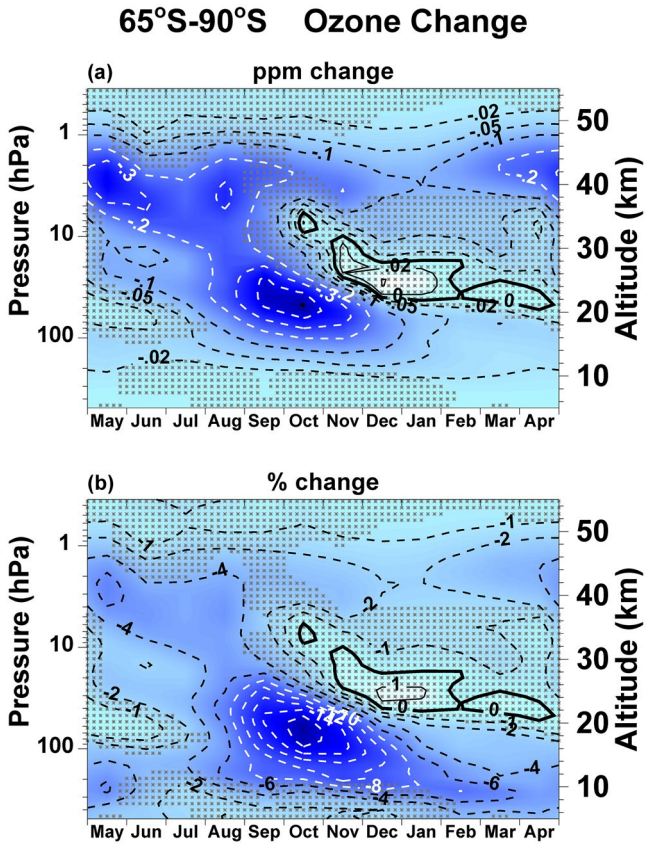

Figure 6. Season (May–April) versus altitude ozone difference (high CFC-11 scenario - baseline) for the Antarctic (65°S-90°S) averaged over 2080–2100, expressed in (a) ppm, and (b) percent. The contours are: (a) ±0.1 ppm and includes the ±0.02 and ± 0.05 contours; (b) ±2% and includes the ±1% contours. Nonshaded regions indicate the response is statistically significant at the 95% level. CFC-11, trichlorofluoromethane.

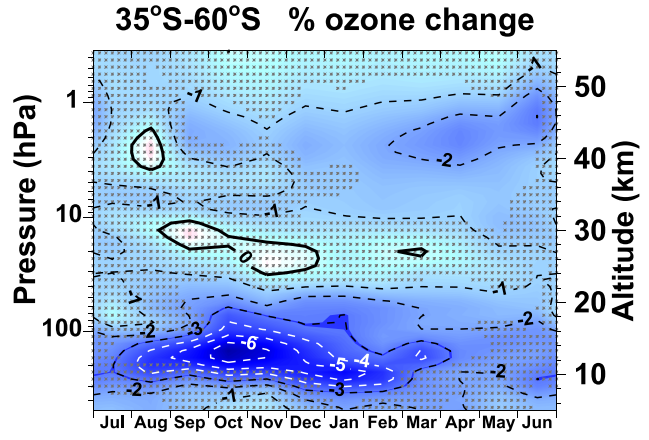

Figure 7. Season (July–June) versus altitude ozone percent difference (high CFC-11 scenario -baseline) for 35°S–60°S averaged over 2080–2100. The contours are ±1%. Nonshaded regions indicate the response is statistically significant at the 95% level. CFC-11, trichlorofluoromethane.

In the Arctic, the high CFC-11 scenario results in additional ozone depletion of 1%–4% (0.05–0.3 ppm) throughout much of the stratosphere during most of the year (Figure 8). However, given the large interannual variability of this region, only small areas are statistically significant at the 95% confidence level. These occur in the upper stratosphere during spring through early winter (May through November), and in the lower stratosphere (20–25 km) only during late spring-early summer (April through July). As noted above, almost no changes in Arctic total column ozone were statistically significant at the 95% level in Figure 4.

3.2. Ozone Depletion Impact on Temperature and Circulation

The additional ozone depletion shown in Figures 2–8 will subsequently reduce the solar UV heating and result in lower temperatures in certain regions of the stratosphere. This effect may be important in the upper stratosphere where the additional ozone loss is significant globally (Figure 5), and heating via solar UV absorption by ozone is a maximum (e.g., Aquila et al., 2016; Fels et al., 1980; Langematz et al., 2003; Ramaswamy et al., 2001; Randel et al., 2017; Shepherd and Jonsson, 2008; Shine et al., 2003; Stolarski et al., 2010). Figure 9a shows the ozone change averaged over 40–50 km (3–0.75 hPa). Ozone depletion is present at all latitudes throughout the year, almost all of which is statistically significant at the 95% level. Additional ozone depletion of ~0.05–0.1 ppm occurs at low-mid latitudes, with larger changes of up to −0.1 to −0.2 ppm at high latitudes. However, while the corresponding temperature change shows net cooling at most latitudes and seasons (Figure 9b), only small regions are statistically significant at the 95% level, with cooling of ~0.2–0.4 K. These tend to occur at mid-latitudes during the spring and summer months when the heating rate is largest and the background variability is weakest. There are also regions of warming which are not statistically significant. These are likely related to interannual dynamical variability which dominates over the relatively smaller UV-ozone heating-induced temperature decreases.

As established in previous observational and modeling studies, ozone depletion and the subsequent reduction in UV heating is the primary driver of past multi-decadal temperature changes in the SH polar lower stratosphere during spring and summer (e.g., Keeble et al., 2014; McLandress et al., 2011; Polvani et al., 2011; Ramaswamy et al., 1996; Randel et al., 2017; Randel and Wu, 1999; Shine, 1986; Solomon et al., 2017; Stolarski et al., 2010; Young et al., 2013). The temperature impact of the deepening ozone hole due to additional CFC-11 is shown in Figure 10a (high CFC-11 – base) averaged over 2080–2100. Here we show the 15 October–15 February average as representative of spring/summer. An area of strong cooling of up to 1.5 K occurs poleward of 50°S at ~300–30 hPa, which is statistically significant at the 95% level. The reduced heating and lower temperatures in the high CFC-11 simulation also increase the area within the polar cap (50°S–90°S) that falls below the 195K threshold for the formation of type I (NAT) PSCs (e.g., Douglass & Fioletov, 2010; Dameris & Godin-Beekmann, 2014). Figure 11a shows this increase in areal coverage of 1%–3% in late May and June, and 3%–7% in August–September in the lower-mid stratosphere. There is also an increase in the area that falls below the 188K threshold for type II ice PSC formation (Figure 11b). This areal increase is a maximum of 3%–5% during August and September (Figure 11b). The temperature changes in Figure 11 tend to

21698996, 2021, 9, Downloaded from https://agupubs.onlinelibrary.wiley.com/doi/10.1029/2020JD033656 by University Of Maryland, Wiley Online Library on [20/01/2023]. See the Terms and Conditions (https://onlinelibrary.wiley.com/terms-and-conditions) on Wiley Online Library for rules of use; OA articles are governed by the applicable Creative Commons License

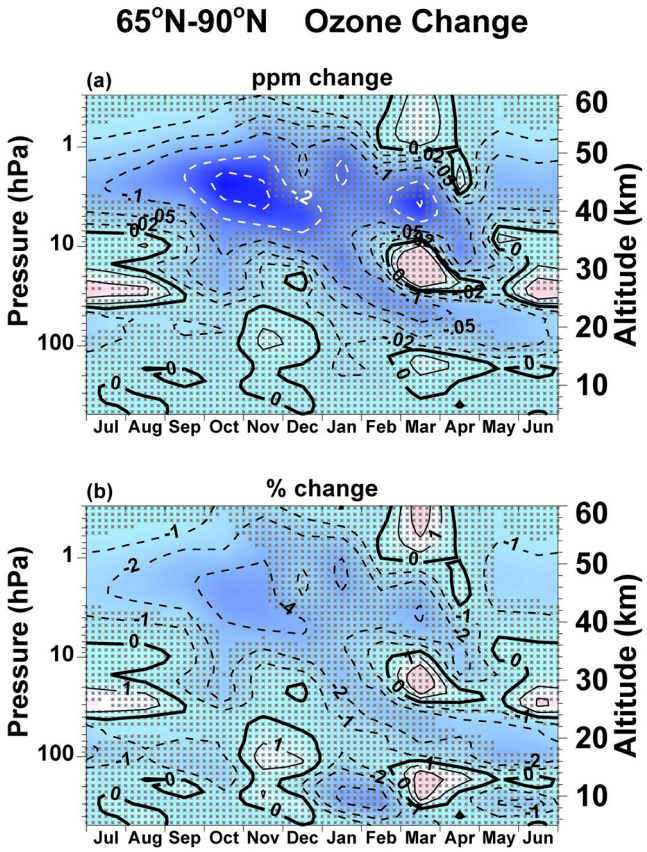

Figure 8. Season (July–June) versus altitude ozone difference (high CFC-11 scenario - baseline), for the Arctic (65°N–90°N) averaged over 2080–2100, expressed in (a) ppm, and (b) percent. The contours are: (a) ±0.1 ppm and includes the ±0.02 and ± 0.05 contours; (b) ±2% and includes the ±1% contours. Nonshaded regions indicate the response is statistically significant at the 95% level. CFC-11, trichlorofluoromethane.

follow the relative magnitude of incident solar radiation and UV-ozone heating, i.e., smallest in June–July and largest in early and late winter (May, August–September). The reduced UV heating and lower temperatures caused by the CFC-11-induced ozone depletion enhance the heterogeneous chlorine activation and ozone loss, and this feedback further deepens the ozone hole as seen in Figures 2–6.

Through thermal wind balance, these temperature changes will also alter the zonal wind and circulation characteristics of the stratosphere (e.g., Arblaster & Gillett, 2014; Langematz et al., 2003; McLandress et al., 2010; Orr et al., 2012; Waugh et al., 1999). The polar lower stratospheric cooling in Figure 10a results in an acceleration of the circumpolar zonal wind throughout the SH polar stratosphere, a good part of which is statistically significant at the 95% level (Figure 10b). Zonal wind accelerations of up to 2 m/sec occur at 70°S, 30 hPa in the 15 October–15 February average (Figure 10b), with maximum accelerations of 3–5 m/sec during 15 October–15 November.

The zonal wind acceleration in the high CFC-11 scenario results in a delay in the spring breakup of the SH polar vortex. To quantify this, we follow previous studies that developed vortex-following diagnostics based on potential vorticity (PV) and zonal wind (Nash et al., 1996; Waugh et al., 1999). Waugh et al. (1999) found very similar year-to-year variations among the diagnostics tested when applied to reanalysis data sets, and concluded that either of the PV or zonal wind diagnostics can be used to quantify the variability in the vortex breakup. Here, we define the breakup date using the zonal wind area diagnostic at 50 hPa (Waugh et al., 1999). Specifically, the vortex breakup is defined to occur when the total area where the zonal wind exceeds 25 m/sec, falls below the area enclosed by 75° equivalent latitude. If this criterion occurs on more than one date in the spring of a particular year, we use the final date of occurrence as the breakup date for that year. Figure 12a shows the annual dates of the breakup of the SH vortex for each year, 2080–2099, for the baseline (blue) and high CFC-11 scenario (red). In the high scenario, the SH vortex has a later breakup date

21698996, 2021, 9, Downloaded from https://agupubs.onlinelibrary.wiley.com/doi/10.1029/2020JD033656 by University Of Maryland, Wiley Online Library on [20/01/2023]. See the Terms and Conditions (https://onlinelibrary.wiley.com/terms-and-conditions) on Wiley Online Library for rules of use; OA articles are governed by the applicable Creative Commons License

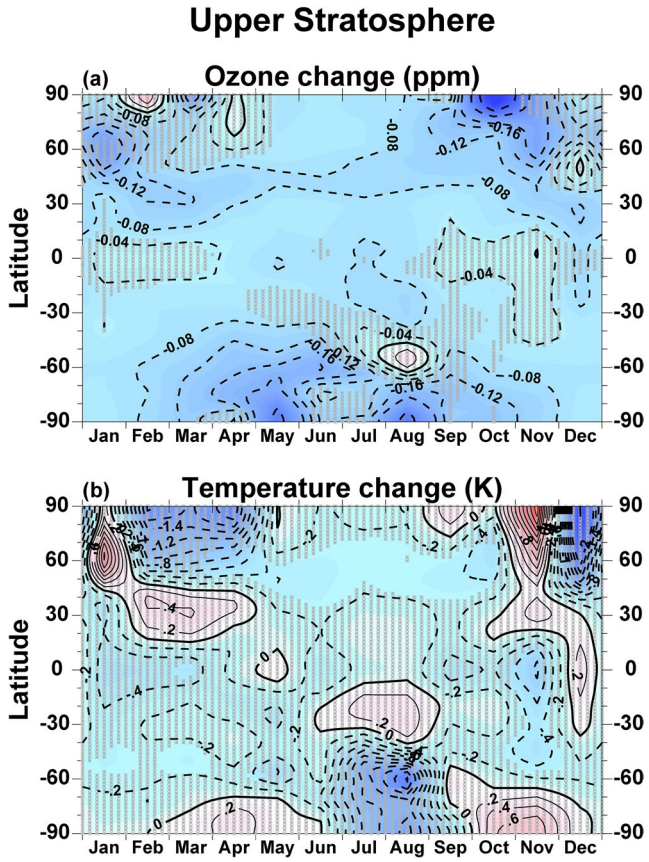

Figure 9. Difference (high CFC-11 scenario - baseline) in the upper stratosphere averaged over 3–0.75 hPa (~40–50 km), for (a) ozone mixing ratio (ppm), and (b) temperature (K). Values are averaged over 2080–2100. The contour intervals are: (a) ±0.04 ppm; (b) ±0.2 K. Nonshaded regions indicate the response is statistically significant at the 95% level. CFC-11, trichlorofluoromethane.

in 14 out of the 20 years. The 20 year average delay relative to the baseline is 4 days (day 332.1 vs. day 328.1; dotted lines in Figure 12), which is statistically significant at the 90% confidence level (but not the 95% level). This is generally consistent with previous model studies that showed a delay in the SH vortex breakup due to diabatic cooling associated with the ozone hole (e.g., Langematz et al., 2003; McLandress et al., 2010; Wilcox & Charlton-Perez, 2013).

In contrast, the Arctic winter and spring stratosphere exhibit large interannual variability, so that any ozone depletion and subsequent temperature and zonal wind change caused by the additional CFC-11 does not have a detectable impact on the timing of the NH polar vortex breakup. In fact, the NH vortex has an *earlier* breakup date in the high CFC-11 scenario in 13 out of 20 years during 2080–2099 (Figure 12b). The NH vortex breakup is advanced by an average of 6.3 days (day 89.9 vs. day 96.2 for the baseline) during 2080–2099, but this is not statistically significant given the large interannual variability in the NH.

The ozone depletion caused by enhanced CFC-11 also changes the SH BDC. Changes in the zonal mean temperature and wind modify the planetary and gravity wave propagation through the SH stratosphere (e.g., Keeble et al., 2014; Li et al., 2008; McLandress et al., 2010; Oberländer et al., 2013; Orr et al., 2012; Shaw et al., 2011). The SH difference in the wave-forced drag on the zonal mean flow, as represented by the Eliassen-Palm (E-P) flux divergence (Andrews et al., 1987), is shown for resolved waves in Figure 13, averaged over 2080–2099. Here, the average is taken over 15 October–15 November to emphasize the seasonal maximum in the difference. Differences in the E-P flux divergence are largest in the SH mid-high latitude upper stratosphere, with values of −0.4 to −0.8 m/sec/day. The difference in wave drag from resolved and unresolved waves causes an enhanced acceleration of the meridional BDC in the high CFC-11 scenario. This is represented by the streamlines in Figure 10a, depicting the difference (high CFC-11 minus base) in the model residual mean meridional and vertical winds of the Transformed Eulerian-Mean formulation (e.g., Andrews et al., 1987; Butchart, 2014). The descent in the polar SH mid-upper stratosphere is increased by 10%–20% in the high CFC-11 scenario, resulting in adiabatic warming and a temperature anomaly of +0.4–0.8 K at ~30–45 km for the 15 October–15 February average (Figure 10a). This polar temperature increase reaches a maximum of +1–2 K during November–December. The associated increased ascent in the SH sub-tropical and mid-latitude stratosphere (20°S–45°S) causes adiabatic cooling, although the corresponding temperature decrease is not statistically significant (Figure 10a).

The dynamical response to the Antarctic ozone hole has been discussed in previous GCM and CCM studies (Austin, 2002; Kiehl et al., 1988; Langematz et al., 2003; Mahlman et al., 1994; Manzini et al., 2003; Stolarski et al., 2006; Smith et al., 2010). A similar feature has also been seen in observational data sets. In an analysis of long term radiosonde data, Randel and Wu (1999) observed Antarctic warming in the mid-stratosphere (30 hPa) from the 1970s to the ~mid-1990s during spring, coincident with large depletion in the ozone hole region. Changes in the BDC depicted in Figure 10a will also drive changes in stratospheric constituents. For example, as noted in Section 3.1, the enhanced Brewer-Dobson descent in the polar mid-upper stratosphere in the high CFC-11 scenario causes a small ozone increase of 0.05–0.1 ppm at 25–35 km in the SH polar cap during November–January (Figure 6). This is consistent with observed ozone changes driven by wave-mean flow interactions (Stolarski et al., 2006).

The ozone depletion caused by enhanced CFC-11 drives an accelerated BDC that then causes small reductions in the stratospheric age of air. Changes in age of air appear statistically from multi-year accumulation of changes in the wave-forcing of the BDC. In much of the stratosphere, differences in the E-P flux divergence and BDC

21698996, 2021, 9, Downloaded from https://agupubs.onlinelibrary.wiley.com/doi/10.1029/2020JD033656 by University Of Maryland, Wiley Online Library on [20/01/2023]. See the Terms and Conditions (https://onlinelibrary.wiley.com/terms-and-conditions) on Wiley Online Library for rules of use; OA articles are governed by the applicable Creative Commons License

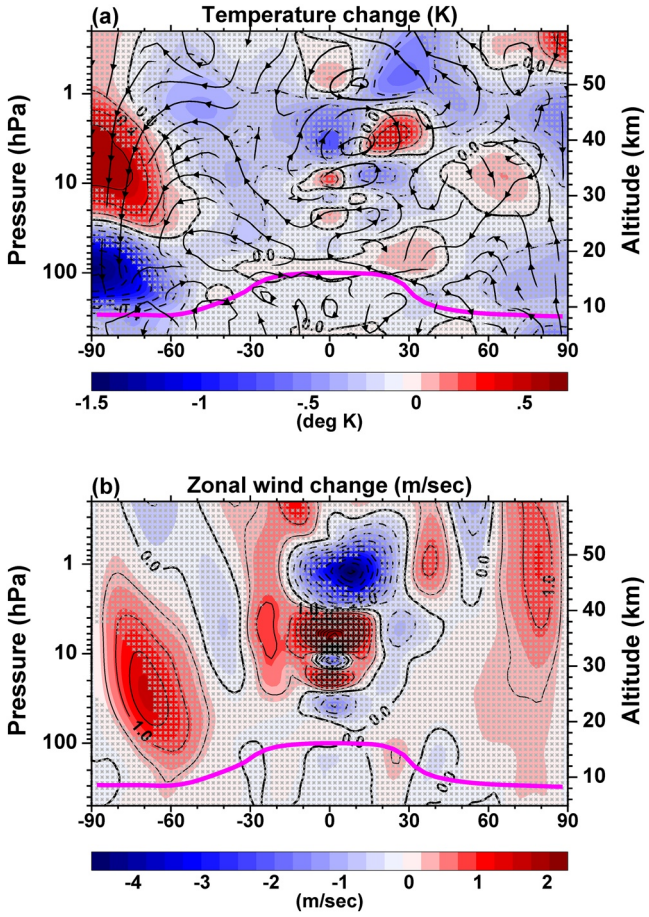

Figure 10. 15 October–15 February average difference (high CFC-11 scenario - baseline) for (a) temperature (K), and (b) zonal wind (m/sec), averaged over 2080–2100. The contour intervals are: (a) ±0.2 K; (b) ±0.5 m/sec. The black streamlines in (a) depict the difference in the residual mean meridional circulation. Nonshaded regions indicate the response is statistically significant at the 95% level. CFC-11, trichlorofluoromethane.

vary widely from year to year and do not show a clear signal in response to the additional CFC-11 prior to ~2090. However, statistically significant differences emerge in the final ~10 years (2090–2099) when the additional CFC-11 has the largest impact. Differences in the E-P flux divergence reach maxima in the mid-upper stratosphere of −0.1 m/sec/day at 40°S–75°S, and −0.1 to −0.3 m/sec/day at 40°N–75°N. Age of air is shown in Figure 14 for the 2090–2099 average baseline (a) and difference, high CFC-11 minus baseline (b). Most of the stratosphere and lower mesosphere is characterized by small age of air decreases (<−0.05 years) which are not statistically significant. Regions of slightly larger changes (−0.05 to −0.1 years) that are statistically significant at the 95% confidence level occur in the SH mid-latitudes near 30 km, and the NH mid-high latitudes at 20–25 km. These regions are generally similar to the maxima in the annual mean age response due to past ODS loading reported in Polvani et al. (2018). Figure 14b also shows an area of small but statistically significant age decrease of up to −0.05 years in the SH mid-latitude lower mesosphere (50–60 km).

We note that the temperature and circulation changes shown in Figures 10–14 are driven predominately by CFC-11-induced ozone depletion. The GHG impacts of CFC-11 will be examined in the next section.

3.3. CFC-11 Greenhouse Gas Impact

To examine the impact of CFC-11 as a GHG, we compare baseline and CFC-11 perturbation simulations from the coupled atmosphere-ocean GEOSCCM described in Section 2. Figure 15 shows the resulting temperature and water vapor responses scaled to the year 2100 CFC-11 perturbation in Figure 1b (125 ppt), as discussed in Section 2. The temperature response has a tropospheric distribution similar to that due to other major GHGs, with maximum warming in the tropical upper troposphere (e.g., Stolarski et al., 2010). However, the responses are small, with a maximum tropospheric warming of 0.08 K, and slight cooling of 0.01–0.02 K throughout much of the stratosphere. The water vapor response is positive everywhere, and also maximizes in the tropical upper troposphere (+2.5%), with increases of ~0.5% throughout the stratosphere. The corresponding stratospheric age of air response is also small, with a maximum change of −0.009 years (not shown). This is significantly smaller than the maximum change of −0.05 to −0.1 years driven predominately by ozone depletion (Figure 14).

We present these results to illustrate the small magnitude of the CFC-11 GHG impact, based on the size of the perturbation used in this study (Figure 1). Furthermore, we emphasize that given the small magnitude of these responses in Figure 15, no regions are statistically significant at the 95% confidence level for temperature, H_2O or age of air. Therefore, such responses likely would not be detectable above the background variability.

4. Conclusions

The recent CFC-11 emissions increase reported in Montzka et al. (2018) has prompted the need to examine the stratospheric response of potential emissions continuing into the future. In this study, we document the stratospheric ozone, temperature, and dynamical impacts of a hypothetical future "high" CFC-11 scenario in which the 2013–2016 inferred average emissions of 72.5 Gg/yr are sustained out to 2100. We compare this with the WMO (2018) baseline in which future emissions decay with the bank release rate of 6.4%/year (Carpenter & Daniel, 2018). As there is large uncertainty in future CFC-11

21698996, 2021, 9, Downloaded from https://agupubs.onlinelibrary.wiley.com/doi/10.1029/2020JD033656 by University Of Maryland, Wiley Online Library on [20/01/2023]. See the Terms and Conditions (https://onlinelibrary.wiley.com/terms-and-conditions) on Wiley Online Library for rules of use; OA articles are governed by the applicable Creative Commons License

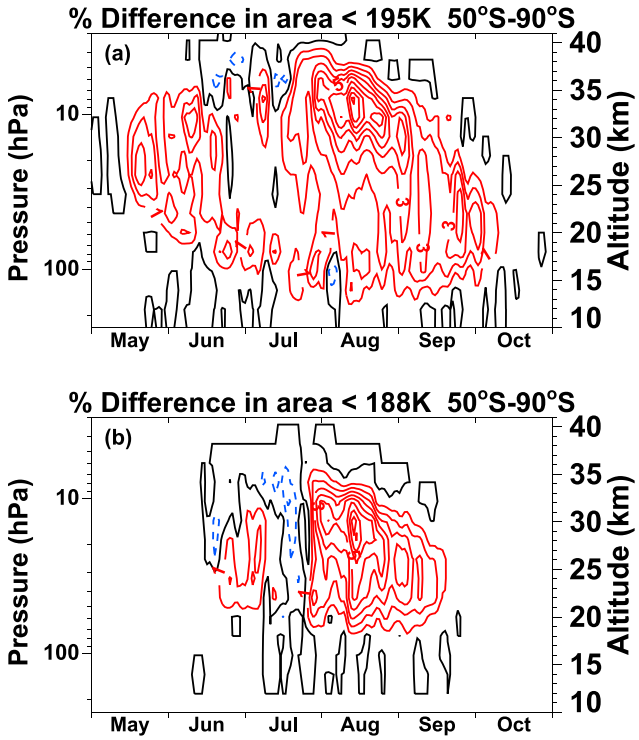

Figure 11. 2080–2099 average percentage difference (high CFC-11 scenario – baseline) in the area within the polar cap (50°S–90°S) that falls below the temperature threshold of: (a) 195K for formation of type I (NAT) PSCs, and (b) 188K for formation of type II (ice) PSCs. The contour interval is ±1%. CFC-11, trichlorofluoromethane; PSC, polar stratospheric cloud.

emissions, the high scenario is not meant to be a realistic projection, but rather tests the sensitivity of the stratospheric ozone and dynamics response. Furthermore, while 72.5 Gg/yr was defined as a "high" scenario based on previous emission estimates, recent findings suggest that future CFC-11 emissions are likely to be substantially higher than previous estimates. This is due to substantially larger bank estimates (Lickley et al., 2020), and potential newly formed banks related to recent unreported production and consumption of CFC-11 in east Asia (Park et al., 2021).

The high scenario significantly perturbs EESC, with a 15% increase above the baseline by 2100. For the 2080–2100 period, there are limited regions where the additional ozone depletion is statistically significant (95% level), and therefore likely detectable above the background variability. These occur in the Antarctic spring lower stratosphere associated with a deepening ozone hole (10%–15% additional depletion), the very lower stratosphere at SH mid-latitudes in spring/summer (4%–6%), and in the upper stratosphere globally (1%–4%). Statistically significant additional ozone depletion (2%–6%) also occurs throughout the year in the SH polar lower stratosphere at 10–20 km and in the total column. In the tropics and NH mid-latitudes, total ozone changes were generally small and not statistically significant at the 95% confidence level. In the Arctic late winter and spring, the relatively large additional total ozone depletion (6%–10%) was not statistically significant given the large interannual variability inherent in this region. Similar regional ozone responses were obtained in other recent modeling studies (Dameris et al., 2019; Fleming et al., 2020; WMO, 2021).

As shown in previous studies, the ozone changes have a mostly linear dependence on the cumulative CFC-11 emissions through the 21st century. In this study, the 2017–2100 average GEOSCCM sensitivity is −0.37 DU per 1,000 Gg and −3.9 DU per 1,000 Gg for global/annual and Antarctic spring total ozone, respectively. This is generally within the middle of the range of other model results reported recently (Dhomse et al., 2019; Fleming et al., 2020; Keeble et al., 2020). Since there is large uncertainty in projecting future emissions, this sensitivity provides a relatively simple metric for estimating the ozone depletion for a given emission scenario.

The impact of additional CFC-11 on the timing of the global ozone recovery is difficult to discern in the simulations presented here. Because of the relatively early return date to 1980 levels in the baseline (2033), which is prior to the time period when the additional CFC-11 emissions have a significant impact, the return to 1980 global ozone levels is delayed by only 1 year in the high CFC-11 scenario (2034). However, for Antarctic spring total ozone, the impact on the recovery is significant, as the return to 1980 levels is delayed by 33 years (2092 vs. 2059).

As is well documented in previous studies, ozone depletion and the subsequent reduction in UV heating drives a response in stratospheric temperature and circulation. The dynamical changes presented here are mostly as expected qualitatively, although they tend to be small given the magnitude of the imposed CFC-11 perturbation, with limited areas where the response is significant and detectable above the background variability. The deepened ozone hole results in a maximum (and statistically significant) temperature change of −1.5 K in the Antarctic lower stratosphere in spring/early summer. Through thermal wind balance, this temperature change causes an acceleration of the circumpolar jet and a marginally significant delay of 4 days in the breakup of the SH polar vortex averaged over 2080–2100. The change in the zonal wind structure also modifies the planetary and gravity wave propagation and E-P flux divergence in the stratosphere. This in turn accelerates the BDC and causes a positive temperature anomaly in the SH polar middle and upper stratosphere, with a maximum response of +2 K in early summer.

21698996, 2021, 9, Downloaded from https://agupubs.onlinelibrary.wiley.com/doi/10.1029/2020JD033656 by University Of Maryland, Wiley Online Library on [20/01/2023]. See the Terms and Conditions (https://onlinelibrary.wiley.com/terms-and-conditions) on Wiley Online Library for rules of use; OA articles are governed by the applicable Creative Commons License

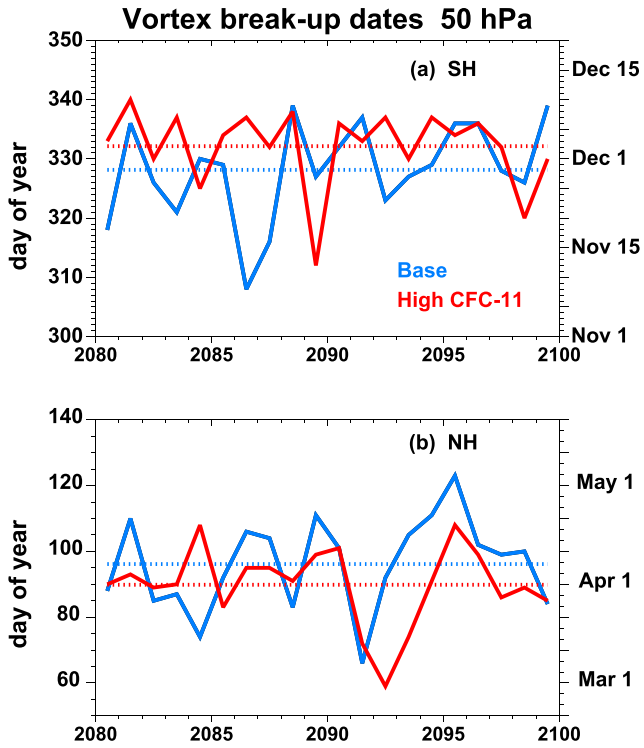

Figure 12. Day of the year of the polar vortex breakup in the (a) SH and (b) NH for the baseline (solid blue) and high CFC-11 scenario (solid red) for 2080–2099. Dotted lines depict the 2080–2099 averages. The breakup date is determined using the zonal wind diagnostic at 50 hPa following Waugh et al. (1999). See text for details. CFC-11, trichlorofluoromethane.

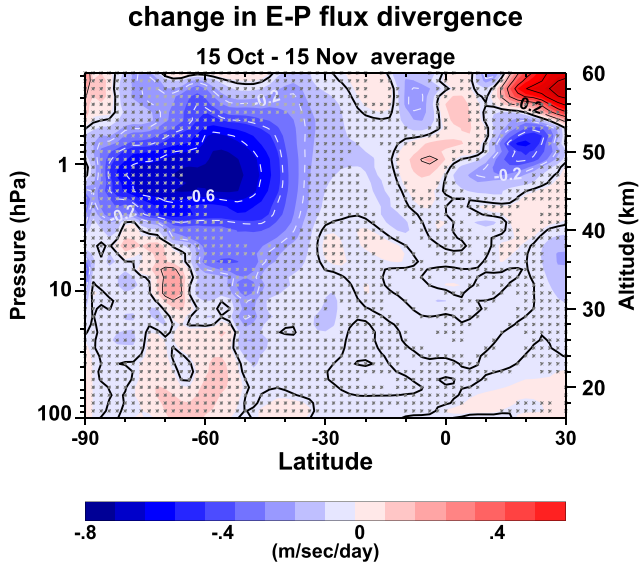

Figure 13. Difference (high CFC-11 scenario – baseline) in the Eliassen-Palm (E–P) flux divergence for resolved waves, averaged over 2080–2099 and 15 October–15 November, for the latitude range 90°S–30°N. The contour interval is ± 0.2 m/sec/day. Nonshaded regions indicate the response is statistically significant at the 95% level. CFC-11, trichlorofluoromethane.

21698996, 2021, 9, Downloaded from https://agupubs.onlinelibrary.wiley.com/doi/10.1029/2020JD033656 by University Of Maryland, Wiley Online Library on [20/01/2023]. See the Terms and Conditions (https://onlinelibrary.wiley.com/terms-and-conditions) on Wiley Online Library for rules of use; OA articles are governed by the applicable Creative Commons License

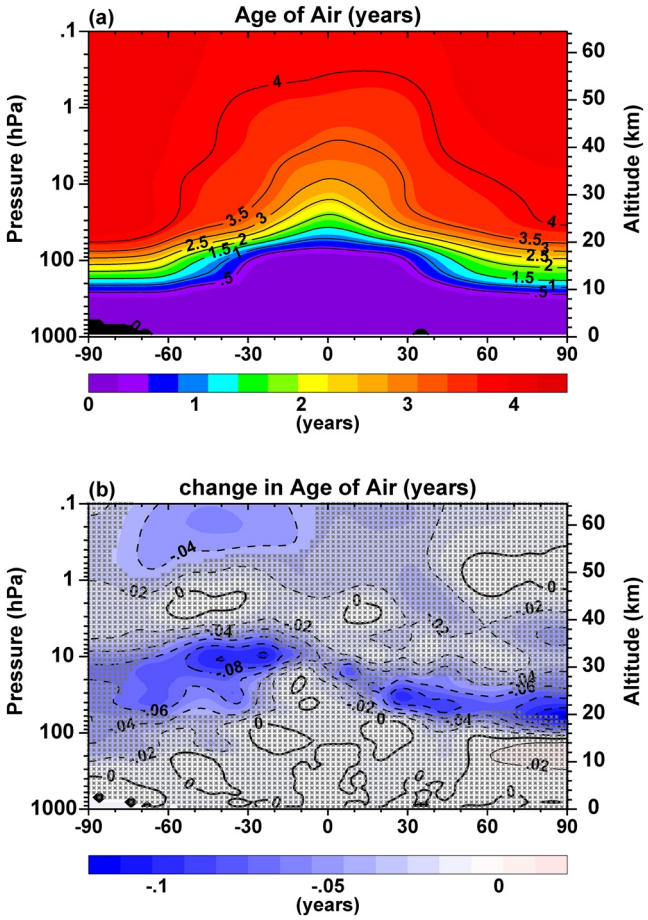

Figure 14. Age of air averaged over 2090–2099 for (a) baseline, and (b) difference, high CFC-11 scenario – baseline. The contour intervals are: (a) ±0.5 years, (b) ±0.02 years. Nonshaded regions in (b) indicate the response is statistically significant at the 95% level. CFC-11, trichlorofluoromethane.

In other regions of the stratosphere, changes in the E-P flux divergence and BDC have large interannual variations and do not show a clear signal until the final 10 years of the simulation (2090–2099) when the additional CFC-11 has the largest impact. Averaged over 2090–2099, the resulting stratospheric age of air was slightly younger globally in the low-mid stratosphere, with maximum changes of −0.1 years which were statistically significant at the 95% confidence level.

To provide a general estimation of the GHG impact of CFC-11, coupled atmosphere-ocean model simulations were performed with a CFC-11 perturbation used in the IR code but not in the ozone chemistry. Assuming the response scales linearly with the CFC-11 perturbation used in this study (125 ppt), the impact was quite small throughout the troposphere and stratosphere, with a radiative forcing of 0.0325 W-m^{-2}. Maximum changes in temperature (+0.08 K) and water vapor (+2.5%) occur in the tropical upper troposphere. Changes in stratospheric age of air were at most −0.009 years, significantly smaller in magnitude than driven by the CFC-11-induced ozone depletion. Furthermore, no regions in the troposphere or stratosphere were statistically significant at the 95% confidence level, so these changes are likely below the limit of detectability.

Finally, we reiterate that while these results are based on one future CFC-11 scenario of continued 72.5 Gg/yr compared with the WMO (2018) baseline, the responses presented here will be roughly proportional to the actual amount of future long-lived chlorinated ODS emissions incurred, based on linearity of the ozone response as shown here and in recent studies.

21698996, 2021, 9, Downloaded from https://agupubs.onlinelibrary.wiley.com/doi/10.1029/2020JD033656 by University Of Maryland, Wiley Online Library on [20/01/2023]. See the Terms and Conditions (https://onlinelibrary.wiley.com/terms-and-conditions) on Wiley Online Library for rules of use; OA articles are governed by the applicable Creative Commons License

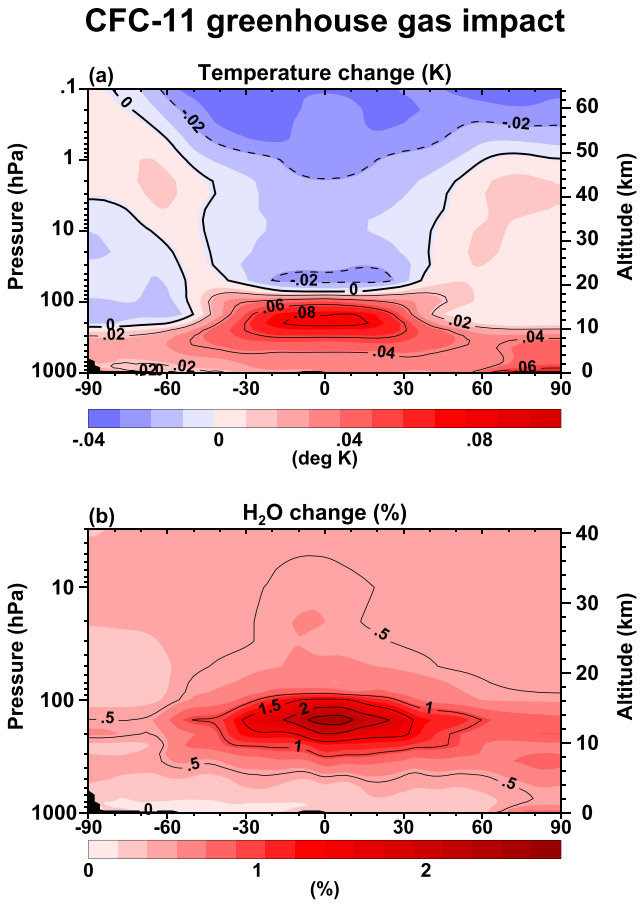

Figure 15. Annual average difference (high CFC-11 scenario - baseline) for (a) temperature (K), and (b) water vapor (%), averaged over the final 10 years of simulations from a coupled atmosphere-ocean version of the GEOSCCM. This depicts the GHG impact of CFC-11: the baseline uses perpetual 1950 conditions for the major GHGs and ODSs (CFC-11 surface mixing ratio is 0.001 ppb); for the high scenario, a CFC-11 perturbation is used in the RRTMG IR code, with the baseline 1950 CFC-11 used in the ozone chemistry (this is otherwise identical to the baseline). See text for details. The contour intervals are: (a) ±0.02 K; (b) ±0.5%. Note that for both panels, no areas are statistically significant at the 95% level. CFC-11, trichlorofluoromethane.

Data Availability Statement

The ground-based total ozone observations used for comparisons are available from https://woudc.org/archive/Projects-Campaigns/ZonalMeans/. Supercomputing resources for GEOSCCM were provided by the NASA High-End Computing (HEC) Program through the NASA Center for Climate Simulation (NCCS) at NASA Goddard Space Flight Center.

Acknowledgments
We thank three anonymous reviewers for helpful comments and suggestions. This work was supported in part by NASA's Atmospheric Composition Modeling and Analysis Program and NASA's Modeling, Analysis, and Prediction Program. GEOSCCM model description, configuration, input parameters and forcing datasets, and associated references are provided in Section 2 of the main text.

References

Andrews, D. G., Holton, J. R., & Leovy, C. B., (1987). *Middle atmosphere dynamics*. 1st Edition, 489, ISBN: 9780080211672. London. Academic Press

Aquila, V., Swartz, W. H., Waugh, D. W., Colarco, P. R., Pawson, S., Polvani, L. M., & Stolarski, R. S. (2016). Isolating the roles of different forcing agents in global stratospheric temperature changes using model integrations with incrementally added single forcings. *Journal of Geophysical Research: Atmospheres*, *121*, 8067–8082. https://doi.org/10.1002/2015JD023841

Arblaster, J. M., & Gillett, N. P. (2014). *Stratospheric ozone changes and climate, chapter 4 of scientific assessment of ozone depletion: 2014, global ozone research and monitoring project, Report No. 55*. Geneva, Switzerland. World Meteorological Organization.

Austin, J. (2002). A three-dimensional coupled chemistry-climate model simulation of past stratospheric trends. *Journal of the Atmospheric Sciences*, *59*, 218–232. https://doi.org/10.1175/1520-0469(2002)059<0218:atdccc>2.0.co;2

Butchart, N. (2014). The Brewer-Dobson circulation. *Reviews of Geophysics*, *52*, 157–184. https://doi.org/10.1002/2013RG000448

Carpenter, L. J., & Daniel, J. S. (2018). *Scenarios and information for policymakers, chapter 6 of scientific assessment of ozone depletion: 2018, global ozone research and monitoring project, Report No.58*. Geneva, Switzerland. World Meteorological Organization.

Chipperfield, M. P., et al. (2014). Multi-model estimates of atmospheric lifetimes of long-lived ozone-depleting substances: Present and future. *Journal of Geophysical Research: Atmospheres*, *119*, 2555–2573. https://doi.org/10.1002/2013JD021097

21698996, 2021, 9, Downloaded from https://agupubs.onlinelibrary.wiley.com/doi/10.1029/2020JD033656 by University Of Maryland, Wiley Online Library on [20/01/2023]. See the Terms and Conditions (https://onlinelibrary.wiley.com/terms-and-conditions) on Wiley Online Library for rules of use; OA articles are governed by the applicable Creative Commons License

Considine, D. B., Douglass, A. R., Connell, P. S., Kinnison, D. E., & Rotman, D. A. (2000). A polar stratospheric cloud parameterization for the global modeling initiative three-dimensional model and its response to stratospheric aircraft. *Journal of Geophysical Research*, *105*, 3955–3973. https://doi.org/10.1029/1999jd900932

Cunnold, D. M., Weiss, R. F., Prinn, R. G., Hartley, D., Simmonds, P. G., Fraser, P. J., et al. (1997). GAGE/AGAGE measurements indicating reductions in global emissions of CCl_3F and CCl_2F_2 in 1992-1994. *Journal of Geophysical Research*, *102*(D1). https://doi.org/10.1029/96jd02973

Dameris, M., & Godin-Beekmann, S. (2014). *Update on polar ozone: Past, present and future, chapter 3 of scientific assessment of ozone depletion: 2014, global ozone research and monitoring project, Report No. 55*. Geneva, Switzerland. World Meteorological Organization.

Dameris, M., Jöckel, P., & Nützel, M. (2019). Possible implications of enhanced chlorofluorocarbon-11 concentrations on ozone. *Atmospheric Chemistry and Physics*, *19*, 13759–13771. https://doi.org/10.5194/acp-19-13759-2019

Dhomse, S., Feng, W., Montzka, S. A., Hossaini, R., Keeble, J., Pyle, J. A., et al. (2019). Delay in recovery of the Antarctic ozone hole from unexpected CFC-11 emissions (2019). *Nature Communications*, *10*, 5781. https://doi.org/10.1038/s41467-019-13717-x

Dhomse, S. S., Kinnison, D., Chipperfield, M. P., Salawitch, R. J., Cionni, I., Hegglin, M. I., et al. (2018). Estimates of ozone return dates from chemistry-climate model initiative simulations. *Atmospheric Chemistry and Physics*, *18*(11), 8409–8438. https://doi.org/10.5194/acp-18-8409-2018

Douglass, A., & Fioletov, V. (2010). *Stratospheric ozone and surface ultraviolet radiation, chapter 2 of scientific assessment of ozone depletion: 2010, global ozone research and monitoring projexxct, Report No. 52*. Geneva, Switzerland. World Meteorological Organization.

Engel, A., & Rigby, M. (2018). *Update on ozone-depleting substances (ODSs) and other gases of interest to the montreal protocol, chapter 1 of scientific assessment of ozone depletion: 2018, global ozone research and monitoring project, Report No.58*. Geneva, Switzerland. World Meteorological Organization.

Eyring, V., Butchart, N., Waugh, D. W., Akiyoshi, H., Austin, J., Bekki, S., et al. (2006). Assessment of temperature, trace species, and ozone in chemistry-climate model simulations of the recent past. *Journal of Geophysical Research*, *111*, D22308. https://doi.org/10.1029/2006JD007327

Eyring, V., Cionni, I., Bodeker, G. E., Charlton-Perez, A. J., Kinnison, D. E., Scinocca, J. F., et al. (2010). Multi-model assessment of stratospheric ozone return dates and ozone recovery in CCMVal-2 models. *Atmospheric Chemistry and Physics*, *10*, 9451–9472. https://doi.org/10.5194/acp-10-9451-2010

Eyring, V., Cionni, I., Lamarque, J. F., Akiyoshi, H., Bodeker, G. E., Charlton-Perez, A. J., et al. (2010). Sensitivity of 21st century stratospheric ozone to greenhouse gas scenarios. *Geophysical Research Letters*, *37*, L16807. https://doi.org/10.1029/2010GL044443

Eyring, V., Lamarque, J.-F., Hess, P., Arfeuille, F., Bowman, K., Chipperfield, M. P., et al. (2013). Overview of IGAC/SPARC chemistry-climate model initiative (CCMI) community simulations in support of upcoming ozone and climate assessments. *SPARC Newsletter*, *40*, 48–66.

Eyring, V., Waugh, D. W., Bodeker, G. E., Cordero, E., Akiyoshi, H., Austin, J., et al. (2007). Multimodel projections of stratospheric ozone in the 21st century. *Journal of Geophysical Research*, *112*, D16303. https://doi.org/10.1029/2006JD008332

Fels, S. B., Mahlman, J. D., Schwarzkopf, M. D., & Sinclair, R. W. (1980). Stratospheric sensitivity to perturbations in ozone and carbon dioxide: Radiative and dynamical response. *Journal of the Atmospheric Sciences*, *37*, 2265–2297. https://doi.org/10.1175/1520-0469(1980)037<2265:SSTPIO>2.0.CO;2

Fioletov, V. E., Bodeker, G. E., Miller, A. J., McPeters, R. D., & Stolarski, R. (2002). Global ozone and zonal total ozone variations estimated from ground-based and satellite measurements. *Journal of Geophysical Research: Atmospheres*, *107*(D22), 4647. https://doi.org/10.1029/2001JD001350

Fleming, E. L., Newman, P. A., Liang, Q., & Daniel, J. S. (2020). The impact of continuing CFC-11 emissions on stratospheric ozone. *Journal of Geophysical Research: Atmospheres*, *125*, e2019JD031849. https://doi.org/10.1029/2019jd031849

Griffies, S. M. (2010). *Elements of MOM4p1 GFDL ocean group technical forestry Report No 6*, 444. Retrieved from https://gfdl.noaa.gov/cms-filesystemaction/model_development/ocean/momguide4p1.pdf

Hansen, J., Sato, M., Ruedy, R., Nazarenko, L., Lacis, A., Schmidt, G. A., et al. (2005). Efficacy of climate forcings. *Journal of Geophysical Research*, *110*, D18104. https://doi.org/10.1029/2005JD005776

Harris, N. R. P., & Wuebbles, D. J. (2014). *Scenarios and information for policymakers, chapter 5 of scientific assessment of ozone depletion: 2014, global ozone research and monitoring project, Report No.55*. Geneva, Switzerland. World Meteorological Organization.

Hurwitz, M. M., Oman, L. D., Newman, P. A., & Song, I.-S. (2013). Net influence of an internally generated quasi-biennial oscillation on modelled stratospheric climate and chemistry. *Atmospheric Chemistry and Physics*, *13*, 12187–12197. https://doi.org/10.5194/acp-13-12187-2013

Iacono, M. J., Mlawer, E. J., Clough, S. A., & Morcrette, J.-J. (2000). Impact of an improved longwave radiation model, RRTM, on the energy budget and thermodynamic properties of the NCAR community climate model, CCM3. *Journal of Geophysical Research*, *105*, 14873–14890. https://doi.org/10.1029/2000jd900091

Keeble, J., Abraham, N. L., Archibald, A. T., Chipperfield, M. P., Dhomse, S., Griffiths, P. T., & Pyle, J. A. (2020). Modelling the potential impacts of the recent, unexpected increase in CFC-11 emissions on total column ozone recovery. *Atmospheric Chemistry and Physics*, *20*, 7153–7166. https://doi.org/10.5194/acp-20-7153-202

Keeble, J., Braesicke, P., Abraham, N. L., Roscoe, H. K., & Pyle, J. A. (2014). The impact of polar stratospheric ozone loss on Southern Hemisphere stratospheric circulation and climate. *Atmospheric Chemistry and Physics*, *14*, 13705–13717. https://doi.org/10.5194/acp-14-13705-2014

Kiehl, J. T., Boville, B. A., & Briegleb, B. P. (1988). Response of a general circulation model to a prescribed Antarctic ozone hole. *Nature*, *332*, 501–504. https://doi.org/10.1038/332501a0

Langematz, U., Kunze, M., Krüger, K., Labitzke, K., & Roff, G. L. (2003). Thermal and dynamical changes of the stratosphere since 1979 and their link to ozone and CO_2 changes. *Journal of Geophysical Research: Atmospheres*, *108*(D1), ACL 9-1-ACL 9-13. https://doi.org/10.1029/2002jd002069

Lean, J., Rottman, G., Harder, J., & Kopp, G. (2005). SORCE contributions to new understanding of global change and solar variability. *Solar Physics*, *230*, 27–53. https://doi.org/10.1007/s11207-005-1527-2

Liang, Q., Stolarski, R. S., Douglass, A. R., Newman, P. A., & Nielsen, J. E. (2008). Evaluation of emissions and transport of CFCs using surface observations and their seasonal cycles and simulation of the GEOS CCM with emissions-based forcing. *Journal of Geophysical Research*, *113*, D14302. https://doi.org/10.1029/2007jd009617

Lickley, M., Solomon, S., Fletcher, S., Velders, G. J. M., Daniel, J., Rigby, M., et al. (2020). Quantifying contributions of chlorofluorocarbon banks to emissions and impacts on the ozone layer and climate. *Nature Communications*, *11*, 1380. https://doi.org/10.1038/s41467-020-15162-7

21698996, 2021, 9, Downloaded from https://agupubs.onlinelibrary.wiley.com/doi/10.1029/2020JD033656 by University Of Maryland, Wiley Online Library on [20/01/2023]. See the Terms and Conditions (https://onlinelibrary.wiley.com/terms-and-conditions) on Wiley Online Library for rules of use; OA articles are governed by the applicable Creative Commons License

Li, F., Austin, J., & Wilson, J. (2008). The strength of the Brewer-Dobson circulation in a changing climate: Coupled chemistry-climate model simulations. *Journal of Climate*, *21*(1), 40–57. https://doi.org/10.1175/2007JCLI1663.110.1175/2007jcli1663.1

Li, F., Newman, P., Pawson, S., & Perlwitz, J. (2018). Effects of greenhouse gas increase and stratospheric ozone depletion on stratospheric mean age of air in 1960-2010. *Journal of Geophysical Research: Atmospheres*, *123*(4), 2098–2110. https://doi.org/10.1002/2017JD027562

Li, F., Vikhliaev, Y. V., Newman, P. A., Pawson, S., Perlwitz, J., Waugh, D. W., & Douglass, A. R. (2016). Impacts of interactive stratospheric chemistry on Antarctic and Southern Ocean climate change in the Goddard Earth Observing System, version 5 (GEOS-5). *Journal of Climate*, *29*(9), 3199–3218. https://doi.org/10.1175/jcli-d-15-0572.1

Mahlman, J. D., Umscheid, L. J., & Pinto, J. P. (1994). Transport, radiative, and dynamical effects of the Antarctic ozone hole: A GFDL "SKYHI" model experiment. *Journal of the Atmospheric Sciences*, *51*, 489–508. https://doi.org/10.1175/1520-0469(1994)051<0489:tradeo>2.0.co;2

Manzini, E., Steil, B., Brühl, C., Giorgetta, M. A., & Krüger, K. (2003). A new interactive chemistry-climate model: 2. Sensitivity of the middle atmosphere to ozone depletion and increase in greenhouse gases and implications for recent stratospheric cooling. *Journal of Geophysical Research*, *108*(D14), 4429. https://doi.org/10.1029/2002jd002977

McCulloch, A., Ashford, P., & Midgley, P. M. (2001). Historic emissions of fluorotrichloromethane (CFC-11) based on a market survey. *Atmospheric Environment*, *35*(26), 4387–4397. https://doi.org/10.1016/s1352-2310(01)00249-7

McLandress, C., Jonsson, A. I., Plummer, D. A., Reader, M. C., Scinocca, J. F., & Shepherd, T. G. (2010). Separating the Dynamical Effects of Climate Change and Ozone Depletion. Part I: Southern Hemisphere Stratosphere. *Journal of Climate*, *23*, 5002–5020. https://doi.org/10.1175/2010jcli3586.1

McLandress, C., Shepherd, T. G., Scinocca, J. F., Plummer, D. A., Sigmond, M., Jonsson, A. I., & Reader, M. C. (2011). Separating the dynamical effects of climate change and ozone depletion. Part II: Southern Hemisphere troposphere. *Journal of Climate*, *24*, 1850–1868. https://doi.org/10.1175/2010JCLI3958.1

Meinshausen, M., Smith, S. J., Calvin, K., Daniel, J. S., Kainuma, M. L. T., Lamarque, J.-F., et al. (2011). The RCP greenhouse gas concentrations and their extensions from 1765 to 2300. *Climatic Change*, *109*, 213–241. https://doi.org/10.1007/s10584-011-0156-z

Mlawer, E. J., Taubman, S. J., Brown, P. D., Iacono, M. J., & Clough, S. A. (1997). RRTM, a validated correlated-k model for the longwave. *Journal of Geophysical Research*, *102*, 16663–16682. https://doi.org/10.1029/97jd00237

Montzka, S. A., Dutton, G. S., Yu, P., Ray, E., Portmann, R. W., Daniel, J. S., et al. (2018). An unexpected and persistent increase in global emissions of ozone-depleting CFC-11. *Nature*, *557*(7705), 413–417. https://doi.org/10.1038/s41586-018-0106-2

Morgenstern, O., Hegglin, M. I., Rozanov, E., O'Connor, F. M., Abraham, N. L., Akiyoshi, H., et al. (2017). Review of the global models used within phase 1 of the chemistry-climate model initiative (CCMI). *Geoscientific Model Development*, *10*, 639–671. https://doi.org/10.5194/gmd-10-639-2017

Nash, E. R., Newman, P. A., Rosenfield, J. E., & Schoeberl, M. R. (1996). An objective determination of the polar vortex using Ertel's potential vorticity. *Journal of Geophysical Research*, *101*(D5), 9471–9478. https://doi.org/10.1029/96JD00066

Nielsen, J. E., Pawson, S., Molod, A., Auer, B., da Silva, A. M., Douglass, A. R., et al. (2017). Chemical mechanisms and their applications in the Goddard Earth observing system (GEOS) Earth system model. *Journal of Advances in Modeling Earth Systems*, *9*(8), 3019–3044. https://doi.org/10.1002/2017MS001011

Oberländer, S., Langematz, U., & Meul, S. (2013). Unravelling impact factors for future changes in the Brewer-Dobson circulation. *Journal of Geophysical Research: Atmospheres*, *118*, 10296–10312. https://doi.org/10.1002/jgrd5077510.1002/jgrd.50775

Olsen, M. A., Schoeberl, M. R., & Nielsen, J. E. (2007). Response of stratospheric circulation and stratosphere-troposphere exchange to changing sea surface temperatures. *Journal of Geophysical Research*, *112*, D16104. https://doi.org/10.1029/2006JD008012

Orr, A., Bracegirdle, T. J., Hosking, J. S., Jung, T., Haigh, J. D., Phillips, T., & Feng, W. (2012). Possible dynamical mechanisms for Southern Hemisphere climate change due to the ozone hole. *Journal of the Atmospheric Sciences*, *69*, 2917–2932. https://doi.org/10.1175/JAS-D-11-0210.1

Park, S., Western, L. M., Saito, T., Redington, A. L., Henne, S., Fang, X., et al. (2021). A decline in emissions of CFC-11 and related chemicals from eastern China, *590*, 433–437. *Nature*. https://doi.org/10.1038/s41586-021-03277-w

Polvani, L. M., Abalos, M., Garcia, R., Kinnison, D., & Randel, W. J. (2018). Significant weakening of Brewer-Dobsoncirculation trends over the 21st century as a consequence of the Montreal Protocol. *Geophysical Research Letters*, *45*, 401–409. https://doi.org/10.1002/2017GL0753410.1002/2017gl075345

Polvani, L. M., Waugh, D. W., Correa, G. J. P., & Son, S.-W. (2011). Stratospheric ozone depletion: The main driver of twentieth-century atmospheric circulation changes in the Southern Hemisphere. *Journal of Climate*, *24*, 795–812. https://doi.org/10.1175/2010JCLI3772.1

Ramaswamy, V., Chanin, M.-L., Angell, J., Barnett, J., Gaffen, D., Gelman, M., et al. (2001). Stratospheric temperature trends: Observations and model simulations. *Reviews of Geophysics*, *39*(1), 71–122. https://doi.org/10.1029/1999rg000065

Ramaswamy, V., Schwarzkopf, M. D., & Randel, W. J. (1996). Fingerprint of ozone depletion in the spatial and temporal pattern of recent lower-stratospheric cooling. *Nature*, *382*, 616–618. https://doi.org/10.1038/382616a0

Randel, W. J., Polvani, L., Wu, F., Kinnison, D. E., Zou, C.-Z., & Mears, C. (2017). Troposphere-stratosphere temperature trends derived from satellite data compared with ensemble simulations from WACCM. *Journal of Geophysical Research: Atmospheres*, *122*, 9651–9667. https://doi.org/10.1002/2017JD027158

Randel, W. J., & Wu, F. (1999). Cooling of the Arctic and Antarctic polar stratospheres due to ozone depletion. *Journal of Climate*, *12*, 1467–1479. https://doi.org/10.1175/1520-0442(1999)012<1467:cotaaa>2.0.co;2

Rigby, M., Park, S., Saito, T., Western, L. M., Redington, A. L., Fang, X., et al. (2019). Increase in CFC-11 emissions from eastern China based on atmospheric observations. *Nature*, *569*(7757), 546–550. https://doi.org/10.1038/s41586-019-1193-4

Sander, S. P., Abbatt, J., Barker, J. R., Burkholder, J. B., Friedl, R. R., Golden, D. M., et al. (2011). "*Chemical kinetics and photochemical data for use in atmospheric studies*. Evaluation Number 17". Pasadena, CA. JPL Publication 10–6, Jet Propulsion Laboratory. Retrieved from: http://jpldataeval.jpl.nasa.gov

Shaw, T. A., Perlwitz, J., Harnik, N., Newman, P. A., & Pawson, S. (2011). The impact of stratospheric ozone changes on downward wave coupling in the Southern Hemisphere. *Journal of Climate*, *24*(16), 4210–4229. https://doi.org/10.1175/2011JCLI4170.1

Shepherd, T. G., & Jonsson, A. I. (2008). On the attribution of stratospheric ozone and temperature changes to changes in ozone-depleting substances and well-mixed greenhouse gases. *Atmospheric Chemistry and Physics*, *8*, 1435–1444. https://doi.org/10.5194/acp-8-1435-2008

Shine, K. P. (1986). On the modelled thermal response of the Antarctic stratosphere to a depletion of ozone. *Geophysical Research Letters*, *13*, 1331–1334. https://doi.org/10.1029/gl013i012p01331

21698996, 2021, 9, Downloaded from https://agupubs.onlinelibrary.wiley.com/doi/10.1029/2020JD033656 by University Of Maryland, Wiley Online Library on [20/01/2023]. See the Terms and Conditions (https://onlinelibrary.wiley.com/terms-and-conditions) on Wiley Online Library for rules of use; OA articles are governed by the applicable Creative Commons License

Shine, K. P., Bourqui, M. S., Forster, P. M. d. F., Hare, S. H. E., Langematz, U., Braesicke, P., et al. (2003). A comparison of model-simulated trends in stratospheric temperatures. *Quarterly Journal of the Royal Meteorological Society*, *129*, 1565–1588. https://doi.org/10.1256/qj.02.186

Smith, A. K., Garcia, R. R., Marsh, D. R., Kinnison, D. E., & Richter, J. H. (2010). Simulations of the response of mesospheric circulation and temperature to the Antarctic ozone hole. *Geophysical Research Letters*, *37*, L22803. https://doi.org/10.1029/2010gl045255

Solomon, S., Ivy, D., Gupta, M., Bandoro, J., Santer, B., Fu, Q., et al. (2017). Mirrored changes in Antarctic ozone and stratospheric temperature in the late 20th versus early 21st centuries. *Journal of Geophysical Research: Atmospheres*, *122*, 8940–8950. https://doi.org/10.1002/2017JD026719

SPARC. (2013). The lifetimes of stratospheric ozone-depleting substances, their replacements, and related species. Ko, M., et al. (Eds.), *SPARC Rep 6*, WCRP-15/2013. Zurich, Switzerland. SPARC Office.

Stolarski, R. S., Douglass, A. R., Gupta, M., Newman, P. A., Pawson, S., Schoeberl, M. R., & Nielsen, J. E. (2006). An ozone increase in the Antarctic summer stratosphere: A dynamical response to the ozone hole. *Geophysical Research Letters*, *33*, L21805. https://doi.org/10.1029/2006gl026820

Stolarski, R. S., Douglass, A. R., Newman, P. A., Pawson, S., & Schoeberl, M. R. (2010). Relative contribution of greenhouse gases and ozone-depleting substances to temperature trends in the stratosphere: A chemistry-climate model study. *Journal of Climate*, *23*, 28–42. https://doi.org/10.1175/2009jcli2955.1

Velders, G. J. M., Andersen, S. O., Daniel, J. S., Fahey, D. W., & McFarland, M. (2007). The importance of the Montreal Protocol in protecting climate. *Proceedings of the National Academy of Sciences*, *104*(12), 4814–4819. https://doi.org/10.1073/pnas.0610328104

Velders, G. J. M., & Daniel, J. S. (2014). Uncertainty analysis of projections of ozone-depleting substances: Mixing ratios, EESC, ODPs, and GWPs. *Atmospheric Chemistry and Physics*, *14*(6), 2757–2776. https://doi.org/10.5194/acp-14-2757-2014

Waugh, D. W., Randel, W. J., Pawson, S., Newman, P. A., & Nash, E. R. (1999). Persistence of the lower stratospheric polar vortices. *Journal of Geophysical Research*, *104*(D22), 27191–27201. https://doi.org/10.1029/1999jd900795

Wilcox, L. J., & Charlton-Perez, A. J. (2013). Final warming of the Southern Hemisphere polar vortex in high- and low-top CMIP5 models. *Journal of Geophysical Research: Atmospheres*, *118*(6), 2535–2546. https://doi.org/10.1002/jgrd.50254

WMO. (1999). *Scientific assessment of ozone depletion: 1998. Global ozone research and monitoring project, Rep. 44*. Geneva, Switzerland. World Meteorological Organization.

WMO. (2014). *Scientific assessment of ozone depletion: 2014. Global ozone research and monitoring project, Report No. 55*. Geneva, Switzerland. World Meteorological Organization.

WMO. (2018). *Scientific assessment of ozone depletion: 2018. Global ozone research and monitoring project, Report No. 58*. Geneva, Switzerland. World Meteorological Organization.

WMO. (2021). *Report on the unexpected emissions of CFC-11. Global ozone research and monitoring project, Report No. xx*. Geneva, Switzerland: World Meteorological Organization.

Young, P. J., Butler, A. H., Calvo, N., Haimberger, L., Kushner, P. J., Marsh, D. R., et al. (2013). Agreement in late twentieth century Southern Hemisphere stratospheric temperature trends in observations and CCMVal-2, CMIP3, and CMIP5 models. *Journal of Geophysical Research: Atmospheres*, *118*, 605–613. https://doi.org/10.1002/jgrd.50126

21698996, 2021, 9, Downloaded from https://agupubs.onlinelibrary.wiley.com/doi/10.1029/2020JD033656 by University Of Maryland, Wiley Online Library on [20/01/2023]. See the Terms and Conditions (https://onlinelibrary.wiley.com/terms-and-conditions) on Wiley Online Library for rules of use; OA articles are governed by the applicable Creative Commons License